Near infrared overtone ($v_{OH} = 2 \leftarrow 0$) spectroscopy of Ne–H_2O clusters

Michael P. Ziemkiewicz, Christian Pluetzer, Michael Wojcik, Jérôme Loreau, Ad van der Avoird, and David J. Nesbitt

Citation: The Journal of Chemical Physics **146**, 104204 (2017); doi: 10.1063/1.4977061
View online: http://dx.doi.org/10.1063/1.4977061
View Table of Contents: http://aip.scitation.org/toc/jcp/146/10
Published by the American Institute of Physics

Near infrared overtone (v_{OH} = 2 ← 0) spectroscopy of Ne–H_2O clusters

Michael P. Ziemkiewicz,[1,a)] Christian Pluetzer,[1,b)] Michael Wojcik,[1,c)] Jérôme Loreau,[2] Ad van der Avoird,[3] and David J. Nesbitt[1]

[1]*JILA, National Institute of Standards and Technology, University of Colorado and Department of Chemistry and Biochemistry, University of Colorado at Boulder, Boulder, Colorado 80309, USA*
[2]*Service de Chimie Quantique et Photophysique, Université Libre de Bruxelles, 50 av. F.D. Roosevelt, CP 160/09, 1050 Brussels, Belgium*
[3]*Theoretical Chemistry, Institute for Molecules and Materials, Radboud University Nijmegen, Heyendaalseweg 135, 6525 AJ Nijmegen, The Netherlands*

(Received 19 December 2016; accepted 9 February 2017; published online 14 March 2017)

Vibrationally state selective overtone spectroscopy and dynamics of weakly bound Ne–H_2O complexes ($D_0^{(para)}$ = 31.67 cm^{-1}, $D_0^{(ortho)}$ = 34.66 cm^{-1}) are reported for the first time, based on near infrared excitation of van der Waals cluster bands correlating with v_{OH} = 2 ← 0 overtone transitions ($|02^-\rangle \leftarrow |00^+\rangle$ and $|02^+\rangle \leftarrow |00^+\rangle$) out of the *ortho* ($1_{01}$) and *para* ($0_{00}$) internal rotor states of the H_2O moiety. Quantum theoretical calculations for nuclear motion on a high level *ab initio* potential energy surface (CCSD(T)/VnZ-f12 (n = 3,4), corrected for basis set superposition error and extrapolated to the complete basis set limit) are employed for assignment of $\Sigma \leftarrow \Sigma, \Pi \leftarrow \Sigma$, and $\Sigma \leftarrow \Pi$ infrared bands in the overtone spectra, where Σ(K = 0) and Π (K = 1) represent approximate projections (K) of the body angular momentum along the Ne–H_2O internuclear axis. End-over-end tumbling of the *ortho* Ne–H_2O cluster is evident via rotational band contours observed, with band origins and rotational progressions in excellent agreement with *ab initio* frequency and intensity predictions. A clear Q branch in the corresponding $|02^+\rangle^f\Pi(1_{11}) \leftarrow {}^e\Sigma(0_{00})$ *para* Ne–H_2O spectrum provides evidence for a novel *e/f parity-dependent* metastability in these weakly bound clusters, in agreement with *ab initio* bound state calculations and attributable to the symmetry blocking of an energetically allowed channel for internal rotor predissociation. Finally, Boltzmann analysis of the rotational spectra reveals anomalously low jet temperatures ($T_{rot} \approx 4(1)$ K), which are attributed to "evaporative cooling" of weakly bound Ne–H_2O clusters and provide support for similar cooling dynamics in rare gas-tagging studies. *Published by AIP Publishing.* [http://dx.doi.org/10.1063/1.4977061]

I. INTRODUCTION

Noncovalent interactions between molecules, though quite weak compared to covalent bond formation, play a critical role in an extraordinary variety of physical and chemical phenomena ranging from phase transitions to molecular adhesion to protein folding.[1–4] Arguably the simplest examples of non-covalent interactions are seen in van der Waals dimers with rare gas atoms for which the binding can vary over an astounding 5 orders of magnitude from relatively strongly bound species like Ar–H_2O[5] (e.g., $D_0 \approx 100$ cm^{-1}) to exceedingly fragile species[6] such as He_2 ($D_0 \approx 0.000\,80$ cm^{-1}). Though such binding energies are small with respect to room temperature (kT ≈ 208 cm^{-1}), they nevertheless can be of major dynamical significance. Indeed, van der Waals interactions in only slightly more strongly bound species (e.g., N_2–H_2O) may be responsible for transient dimer formation in colder regions of the upper Earth atmosphere, as well as directly influencing metastable structures in a variety of low temperature, non-equilibrium environments such as noble gas matrices,[7] doped helium nanodroplets,[8] and supersonic jets.[9] Furthermore, weak attractive interactions are now thought to play a critical role in stabilizing pre-reactive complexes in the early stages of a chemical reaction.[10] Such interactions have also been speculated to control the degree of solvation for non-polar hydrophobic molecules in water[11] and thus the propensity to produce clathrates under high pressure conditions.[12]

Detailed insights into the intermolecular potential energy surfaces (PESs) associated with these interactions can be obtained via high resolution spectroscopy of strong infrared chromophores such as H_2O complexed with rare gas atoms for which the "supermolecules" are bound non-covalently by combination of (i) van der Waals attraction between two polarizable species and (ii) dipole-induced dipole interaction between a permanent dipole and a polarizable species. In particular, the present work focuses specifically on Ne–H_2O (see Fig. 1), a very weakly bound van der Waals structure in which the presence of shallow minima and low barriers in the potential energy surface allows for extreme large amplitude

[a)]Current address: Vescent Photonics with Analog Devices, 14998 W. 6th Ave. #700, Golden, CO 80401, USA.
[b)]Current address: West Pharmaceutical Services Deutschland GmbH & Co. KG, Stolberger Strasse 21-41, 52249 Eschweiler, Germany.
[c)]Current address: Space Dynamics Laboratory, 1695 North Research Park Way, North Logan, UT 84341, USA.

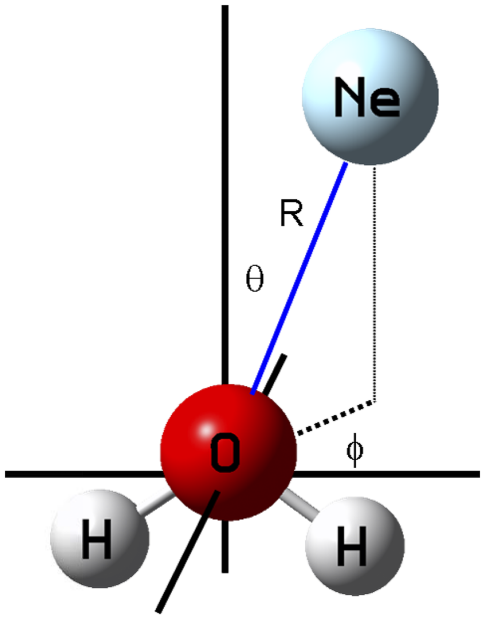

FIG. 1. Ne–H_2O in 3D van der Waals coordinates (R, θ, ϕ) for a fixed vibrationally averaged H_2O geometry. The global minimum in the CCSD(T)-f12b/VnZ-f12 (n = 3,4) potential surface for ground state H_2O, corrected for BSSE and extrapolated to the CBS limit is at E = −63.50 cm^{-1} (R = 3.206 Å, θ = 73.0°, ϕ = 0.0°) with respect to infinite R, with dissociation energies of D_0 = 34.66 cm^{-1} and 31.67 cm^{-1} predicted for *ortho* and *para* Ne–H_2O complexes, respectively.

motion effects. This system is of special dynamical interest, as such clusters facilitate quantum exploration over a significant fraction of the potential energy surface even for the lowest internal rotor states populated at supersonic jet temperatures.

There has been considerable theoretical and experimental interest in the very lightest and most weakly bound van der Waals dimers of H_2O with He and H_2, particularly in efforts to understand transient dimer formation and collisional energy transfer dynamics in the interstellar medium.[13–15] Conversely, the greater ease of formation in cold supersonic jets has motivated exploration of the much heavier and more strongly bound rare gas dimers of H_2O with Ar, Kr, and Xe, based on both direct absorption and vibrationally mediated photolysis (VMP) techniques in the mid, near, and far infrared region.[5,9,16–21] In clear contrast, there has been much less experimental work on Ne–H_2O for which the binding energies ($D_0 \approx 32$ cm^{-1} for *para* H_2O and $D_0 \approx 35$ cm^{-1} for *ortho* H_2O) and large amplitude internal rotor motion are thought to be intermediate between He–H_2O ($D_0 \approx 6.8$ cm^{-1}) and Ar–H_2O ($D_0 \approx 100$ cm^{-1}).[5,22–25] There have been recent high resolution mid infrared spectra reported for Ne–H_2O/D_2O clusters in the HOH/DOD fundamental bend region, which now provide the first high resolution spectroscopic data for the bending manifold.[26,27] However, there have been no experimental reports in the literature of Ne–H_2O spectra in the OH stretch fundamental and/or overtone region, with no studies whatsoever on vibrational predissociation dynamics in these clusters.

Theory has therefore generally taken the lead in this arena. To facilitate the spectroscopic analysis of large amplitude motion in Ne–H_2O van der Waals complexes, potential energy surfaces have been calculated with MP2 theory,[22] with later refinements at the CCSD(T)/aug-cc-pVQZ level.[23,24]. These studies have yielded estimates for equilibrium binding energies (i.e., excluding zero point motion in intermolecular degrees of freedom) of $D_e \approx 67$ cm^{-1} and a barrier to in-plane rotation[24] of ≈17 cm^{-1}. Theoretical studies by Sun *et al.*[27] reported an improved potential energy surface at the CCSD(T)/aug-cc-pVQZ level, implemented with multidimensional quantum calculations to extract many of the bound internal rotor states of Ne–H_2O for multiple (^{20}Ne, ^{22}Ne, ^{16}O, ^{17}O, and ^{18}O) isotopomers. These calculations facilitated simple fits of the *ab initio* energy levels to quasidiatomic rotational progressions, yielding estimates of rotational constants ($B \approx 0.142$ cm^{-1} and $D \approx 1.8 \times 10^{-5}$ cm^{-1}) for the ground state and already in fair agreement ($B = 0.136\ 40$ cm^{-1} and $D = 1.63 \times 10^{-5}$ cm^{-1}) with results recently reported in high resolution spectroscopic studies by Li *et al.*[26] on the isotopically substituted Ne–D_2O system. Finally, studies by Dopfer *et al.*[28] have shed light on the analogous H_2O^+–Ne complex, although stronger non-covalent binding in a molecular ion-based van der Waals species results in much greater potential surface anisotropy and thus potentially rather different internal rotor dynamics than for neutral Ne–H_2O clusters.

Valuable insight can be gained from previous experimental rovibrational studies pursued on a number of cluster systems, specifically H_2–H_2O,[29–32] Kr–H_2O[19], and Xe–H_2O[24], with special emphasis on Ar–H_2O.[5,9,16,17,20] In-plane rotation of the H_2O molecule in Ar–H_2O is hindered by a 26 cm^{-1} barrier,[24] which constitutes only a small change with respect to the $D_e \approx 143$ cm^{-1} equilibrium binding energy. The presence of a small barrier allows for largely free rotational motion, but with angular momentum projection K of H_2O in the dimer frame as an approximate quantum number. These internal rotor states are therefore labeled by K and j_{kakc}, [e.g., $\Sigma(1_{01})$, $\Pi(1_{01})$] to indicate a specific asymmetric top wave function with K = 0 (Σ) or 1(Π) projection of j on the body-fixed intermolecular z-axis. Built on such widely spaced internal rotor structure are (i) progressions in the total angular momentum **J** = **N** + **j**, which arise from the vector sum of internal rotor (**j**) and end-over-end tumbling (**N**) of the Ne–H_2O pseudodiatomic and (ii) 1D vibrational excitation of van der Waals stretching quanta (n) along the center of mass axis, with (iii) rigorous quantum labels for the H_2O nuclear spin state (*ortho*/*para*) and overall parity (*e*/*f*) of the total wavefunction.[33] Due to a much smaller dissociation energy ($D_0 \approx$ 32-35 cm^{-1}), the number of energetically bound internal rotor/van der Waals states for Ne–H_2O is quite small but nevertheless still large enough to be dynamically rich.

In addition to rigorously bound states, there are also metastable resonance states detectable in the overtone IR action spectrum. Of particular dynamical interest in these systems is the capacity to remain intact, despite intramolecular vibrational excitation far in excess of the weak van der Waals bond strength. This can be especially dramatic in rare gas clusters such as Ne–H_2O, where even the lowest energy fundamental bending excitation of the H_2O moiety ($\nu_2 \approx 1600$ cm^{-1}) is already >50-fold greater than the dissociation limit. Due to the metastability of these upper states, such weakly bound van der Waals systems still can, in principle, yield exceptionally high resolution, often Doppler/laser limited infrared

spectra ($\Delta\nu \approx 0.002$ cm^{-1}), i.e., characteristic of $>10^7$ vibrational periods prior to cleavage of the weak van der Waals bond.[17,20,30,34,35]

The goal of the present work is a combined experimental and *ab initio* theoretical study of vibrationally mediated photolysis (VMP) $v_{OH} = 2 \leftarrow 0$ overtone spectroscopy of Ne–H_2O dimers. The organization of this paper will be as follows. Sec. II provides a brief overview of the experimental apparatus, followed in Sec. III by description of the high level *ab initio* and quantum dynamical theoretical methods used to help assign and interpret the observed VMP spectra. Sec. IV contains a presentation of the key experimental results, reporting infrared overtone absorption spectra in the $v_{OH} = 2 \leftarrow 0$ region (specifically $|02^-\rangle \leftarrow |00^+\rangle$ and $|02^+\rangle \leftarrow |00^+\rangle$ in the local mode notation of Child and Lawton[36,37]) for *ortho* and *para* Ne–H_2O dimers. Finally, in Section V, the results are explicitly discussed in comparison with first principles *ab initio* theoretical predictions, with results summarized in Sec. VI.

II. EXPERIMENTAL

The experimental apparatus (see Fig. 2) has been previously discussed in detail;[9,31,38,39] we therefore only briefly summarize aspects of particular relevance to the current Ne–H_2O study. The gas manifold comprises a 1.5 L steel tank of high purity deionized liquid water into which pure neon is bubbled at 4600 torr through a steel aspirator. The tank is held at 0 °C, resulting in a 4.6 torr H_2O vapor pressure and 0.1% H_2O/Ne gas mixture. Trace amounts of H_2O are empirically found to yield maximal Ne–H_2O dimer concentrations, presumably due to competitive production of larger Ne–$(H_2O)_n$ or $(H_2O)_n$ cluster species with increasing H_2O partial pressure. This gas mixture is then introduced via a needle valve at 600 torr backing pressure into the stagnation region of a homemade pulsed slit expansion source (4 cm × 250 μm, 1 ms pulse, 10 Hz rep rate). Typical flow rates at 1% duty cycle are 360 standard cm^3/min, which with a 4500 L/s diffusion pump translates into an average chamber pressure of $\sim 10^{-4}$ torr under full pulsed valve operation.

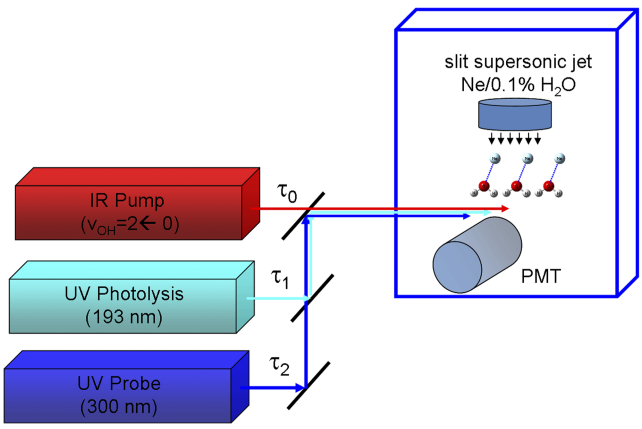

FIG. 2. Experimental schematic of the vibrationally mediated photolysis (VMP) slit jet spectrometer, with spatially overlapping IR pump, UV photolysis, and UV probe laser pulses along the long axis of a slit jet supersonic expansion. Vibrational overtone spectroscopy ($v_{OH} = 2 \leftarrow 0$) and predissociation dynamics of Ne–H_2O can be probed by tuning the IR laser frequency and the pump-photolysis time delay, respectively (see text for details).

The resulting Ne–H_2O van der Waals clusters formed in the supersonic expansion travel ~2 cm through the main chamber to the interaction region, where the gas jet encounters a sequence of three spatially overlapped 8 ns laser pulses (IR-UV-UV) parallel to the long axis of the slit expansion to maximize the interaction path length (see Fig. 2). The first pulse ("IR pump") from a tunable optical parametric oscillator (7210-7300 cm^{-1}, ~15 mJ, 0.20 cm^{-1} resolution) is tuned over the $v_{OH} = 2 \leftarrow 0$ H_2O overtone OH stretch band region to achieve quantum state resolved rovibrational excitation of Ne–H_2O dimer. A second pulse ("UV photolysis") from an ArF excimer laser (193 nm, 15 mJ) arrives after a delay time τ_1, during which time the cluster can predissociate into free Ne + $|01^+\rangle|v_{bend}\rangle$ or $|01^-\rangle|v_{bend}\rangle$ states of the H_2O monomer. This 193 nm photon energy is non-resonant with $\tilde{A}^1B_1 \leftarrow \tilde{X}^1A_1$ excitation out of the ground vibrational state of H_2O, with the photolysis cross section vibrationally enhanced by >10-fold for $v_{OH} = 1$ or higher.[40] Selective photolysis of vibrationally excited H_2O containing species proceeds rapidly on the dissociative $^1B_1$ surface, with the resulting photoejected OH fragments probed by laser induced fluorescence (LIF) with a third pulse ("UV probe") from the frequency doubled output of a DCM dye laser, detected with a 10 ns gated photomultiplier, captured by box car integrator, and digitized in an A/D converter. This LIF laser (~0.1-1 mJ) is in turn tuned over the full OH ($\tilde{A}^2\Sigma \leftarrow \tilde{X}^2\Pi$) band to yield nascent rovibrational, spin orbit, and lambda doublet populations in OH($^2\Pi_{1/2,3/2}$; N; v = 0, 1, or 2). To further minimize background contributions from non-vibrationally mediated photolysis of H_2O clusters, the LIF probe laser is triggered at 5 Hz, with signals actively subtracted in alternating pulse mode. The net result is a high background rejection method for identifying extremely weak rovibrational overtone transitions in H_2O containing cluster species, leveraged by the ≥100-fold vibrationally enhanced 193 nm UV photolysis of H_2O in the initially excited overtone ($v_{OH} = 2$) manifold.

III. *AB INITIO*/QUANTUM DYNAMICAL CALCULATIONS

A. Potential energy surface

Reliable assignment of the experimental bands requires accurate predictions of the relevant internal rotor energy levels in the ground and overtone state. For the purpose of making initial spectroscopic assignments, we have performed fully converged bound state calculations of the lowest internal rotor energy levels on a high level Ne–H_2O potential surface. The Ne–H_2O interaction potential has been calculated *ab initio* by means of the explicitly correlated coupled-cluster method CCSD(T)-f12b implemented in the MOLPRO package[41] with the specially optimized correlation consistent basis sets (VnZ-f12, n = 3,4) of Peterson *et al.*[42] All energies have been corrected for basis set superposition error (BSSE) with the counterpoise (CP) correction method and the individual Hartree-Fock reference, correlation, and perturbative triples (T) energies extrapolated to the complete basis set (CBS) limit.[43,44]

The geometry of the Ne–H_2O complex has been expressed in spherical coordinates (R, θ, and φ) illustrated in Fig. 1. R is the length of the vector **R** connecting Ne to the center of mass

of H_2O, while θ and φ are the polar and azimuthal angles of **R** in a frame with H_2O in the xz plane and the C_2 axis of H_2O along the z-axis. H_2O is kept rigid at its equilibrium geometry with r_{OH} = 0.9587 Å and HOH angle = 104.420°, while the potential energy surface (PES) is constructed from 3276 symmetry-unique geometries. The radial grid consists of 36 points from 2 to 10 Å with spacings of ΔR = 0.1 Å and 1 Å in the intervals R = 2-5 Å and 5-10 Å, respectively. A constant 15° step size is used for the angular grid, with 13 points in θ from [0, π] and 7 points in φ from [0, π/2].

In order to obtain an analytic representation of the PES, we first perform an expansion in tesseral harmonics[45] S_{lm} (θ, φ), i.e., real combinations of spherical harmonics Y_{lm}(θ, φ),

$$V(R,\theta,\varphi) = \sum_{l,m} v_{lm}(R) S_{lm}(\theta,\varphi) \quad (1)$$

with the R-dependent expansion coefficients v_{lm} obtained using Gauss-Legendre and Gauss-Chebyshev quadratures for θ and φ, respectively. For each value of R, the PES is calculated at the quadrature points by performing a cubic spline interpolation in the angular coordinates. The expansion includes all $0 \le l \le 10$ and $0 \le m \le l$, where, due to symmetry, only terms with even m are present.[46] The functions v_{lm}(R) are then interpolated in R using cubic splines. The asymptotic (R > 10 Å) part of the potential has been obtained by fitting each v_{lm}(R) to the expression $-C_6/R^6 - C_8/R^8$, using the outermost three points of the grid.[46] In order to avoid discontinuity problems, we use a switching function that smoothly interpolates between the *ab initio* points and the asymptotic fit, specifically f(R) = [1 + tanh (β(R − R_s))]/2 with parameters β = 1.7 a_0^{-1} and R_s = 17 a_0.

The main features of the resulting Ne–H_2O PES have been investigated and discussed previously[24,27] and are reproduced by our PES. The global minimum corresponds to a coplanar geometry (R = 3.21 Å, θ = 73.0°, and φ = 0°) at E = −63.50 cm^{-1}, which compares quite well with earlier efforts that left out explicit electron correlation effects.[24,27] Two-dimensional cuts of the PES are shown in Figs. 3(a) and 3(b). The cut for φ = 0° in Fig. 3(a) displays the global minimum, as well as the two saddle points for θ = 0° and 180°, which clearly reveal barriers to in-plane rotation.

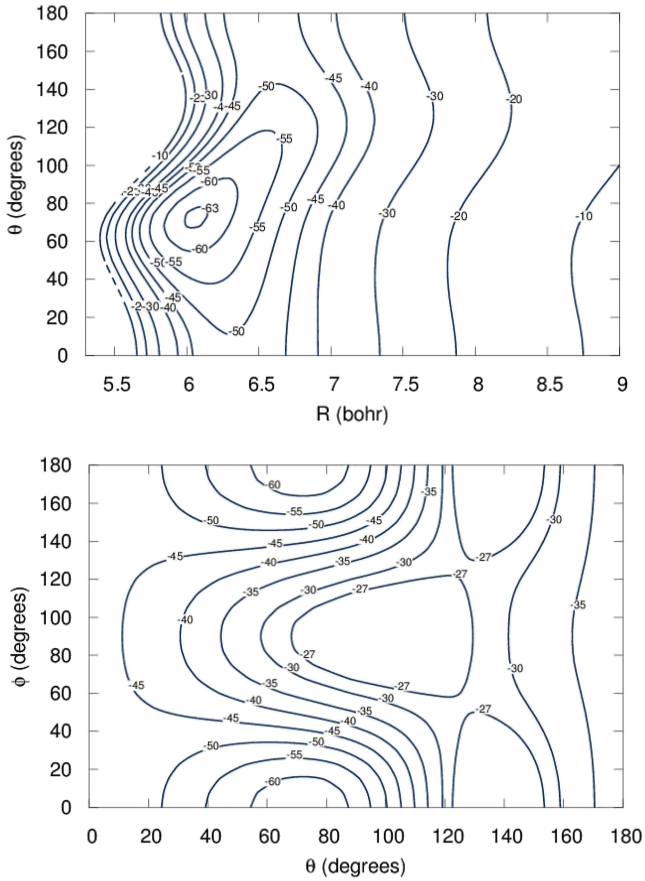

FIG. 3. 2D slices (a): V(R, θ; φ = 0°), (b): V(θ, φ; R = 3.21 Å) through a 3D Ne–H_2O potential energy surface (PES), calculated at the CCSD(T)-f12b level with high level correlation consistent VTZ-f12/VQZ-f12 basis sets, corrected for basis set superposition error (BSSE) with counterpoise corrections, and extrapolated to the complete basis set limit (CBS).[42,43] The minimum in the PES potential energy surface (D_e = −63.50 cm^{-1}) corresponds to a planar geometry with the H_2O a-axis pointing approximately towards the Ne atom (R = 3.206 Å, θ = 73.0°, φ = 0°), but with only modest barriers to both in-plane (≈ 20-30 cm^{-1}) and out of plane (≈ 20 cm^{-1}) internal rotation. Anisotropy in this potential is sufficient to permit internal H_2O motion to be treated as a hindered asymmetric rotor, with well-defined projections (Σ, Π) of j in the body fixed frame for states of low total angular momentum.[32]

B. Bound states

To obtain the bound states of H_2O–Ne, we use the variational approach for van der Waals complexes described extensively in previous work.[32,47] The Hamiltonian of the complex is diagonalized in a basis consisting of products of angular and radial functions. The latter are contracted discrete variable representations (DVRs) calculated using an effective potential of the form V_{eff} (R) = α[V_0(R) + ζR], with the potential V_0(R) cut through the minimum of the PES for θ = 73° and φ = 0°. The parameters α and ζ are optimized by minimizing the energy of the lowest eigenvalue in full three-dimensional calculations for each irreducible representation (irrep) of the symmetry group of the H_2O–Ne complex and total angular momentum J = 0 from which suitably optimum values are found to be α = 0.5 and ζ = 5 × 10^{-4} hartree/a_0. The basis includes angular functions with $j \le 10$ (where j denotes the angular momentum of the free H_2O monomer) and 25 radial functions computed on an equidistant DVR grid of 386 points in the range R = 4.5-35 a_0. The energies of the rovibrational levels are converged to ≤10^{-4} cm^{-1}, with bound states calculated for all values of total angular momentum from J = 0-10.

We compute the bound states corresponding to the four relevant vibrational states of the H_2O monomer (|00$^+$⟩, |02$^+$⟩, |02$^-$⟩, and |11$^+$⟩) on the same intermolecular potential surface, but using different vibrationally averaged, effective rotational constants A_v, B_v, and C_v for H_2O. This is important, since zero point energy in the internal rotor levels and thus shifts in the vibrational band origins can be quite sensitive to these values. As a result, these values are chosen to exactly reproduce the rigid rotor energies of the j_{kakc} = 0_{00}, 1_{01}, 1_{11}, 1_{10} rovibrational states in each vibrational manifold of H_2O (see Table I[48]), as only the lowest H_2O internal rotor levels will be thermally populated in the H_2O–Ne complex.[48]

TABLE I. Vibrational state specific rotational constants[a] for H_2O (in cm^{-1}) used in the bound state calculations.

State	A	B	C
$\|00^+\rangle$	27.8572	14.5145	9.2799
$\|02^+\rangle$	26.3406	14.1137	8.9268
$\|02^-\rangle$	25.9526	14.2101	8.9715
$\|11^+\rangle$	25.5926	14.2986	8.9976

[a]Obtained in the rigid asymmetric top limit from spectroscopic 0_{00}, 1_{01}, 1_{11}, and 1_{10} energy levels.[48]

C. Transitions and intensities

In order to obtain a completely *ab initio* prediction of the spectra, we use the wave functions from the bound state calculations to compute the line strengths of all electric dipole allowed $\Delta J = 0, \pm 1$ transitions between rovibrational states of the H_2O–Ne complex for J = 0-10 that accompany transitions of the H_2O monomer from its vibrational ground state $|00^+\rangle$ to each of the $|02^+\rangle$, $|02^-\rangle$, and $|11^+\rangle$ vibrationally excited states. The molecular symmetry group of the Ne–H_2O complex is $C_{2v}(M)$, which is isomorphic with the point group symmetry of the H_2O monomer.[49] The overall wavefunction symmetry in the complex is determined by (i) the H_2O vibrational state symmetry and (ii) the symmetry of the bound state wave function describing internal and overall rotation of Ne–H_2O. For simplicity, note that the PES (although *not* the kinetic energy operator) is approximated to be independent of H_2O vibrational quantum state, which presumes the upper states to be stable with respect to pure vibrational (but not necessarily internal rotor) predissociation. The vibrational wave functions $|00^+\rangle$, $|02^+\rangle$, and $|11^+\rangle$ of H_2O transform according to irrep A_1 of $C_{2v}(M)$, while the $|02^-\rangle$ vibrational wave function transforms according to irrep B_2. Therefore, the states of the complex with the H_2O monomer in states $|00^+\rangle$, $|02^+\rangle$, and $|11^+\rangle$ have the same overall symmetry as our bound states, while the symmetry of the Ne–H_2O wavefunction with H_2O in the $|02^-\rangle$ state is obtained by multiplying the bound state irreps with the irrep B_2 of the H_2O monomer vibration.

As the spectra reflect transitions in both the *ortho* and *para* H_2O manifolds, we must add nuclear spin wavefunction considerations for the identical H atoms. In general, the Pauli principle requires spatial wave functions of overall A_1 or A_2 symmetry for *para* Ne–H_2O with total proton spin I = 0, with corresponding spatial wave functions of overall symmetry B_1 or B_2 for *ortho* H_2O–Ne with total proton spin I = 1.[49] The overall dipole operator is symmetric under the proton permutation,[50] antisymmetric under inversion E^*, and thus has symmetry A_2. Parallel transitions in the H_2O monomer from the $|00^+\rangle$ ground state to the $|02^+\rangle$, $|11^+\rangle$ vibrational states involve the dipole component μ_z, which has A_1 symmetry, whereas perpendicular transitions to the $|02^-\rangle$ state involve the μ_x component of symmetry B_2. Intermolecular transitions accompanying the transitions to the $|02^+\rangle$ and $|11^+\rangle$ states involve vibrational transition dipole moments $\langle 00^+|\mu_z|11^+\rangle$ parallel to the C_2 axis of H_2O and of symmetry A_2 in the intermolecular coordinates, while the transition to the $|02^-\rangle$ state involves $\langle 00^+|\mu_x|02^-\rangle$ perpendicular to the H_2O symmetry axis and of symmetry B_1 in the intermolecular coordinates. For *para* Ne–H_2O in the vibrational ground state, the intermolecular states must have A_1 or A_2 symmetry. Therefore, the intermolecular excited states in transitions to the $|02^+\rangle$ and $|11^+\rangle$ states must also have A_1 or A_2 symmetry. Similarly, for *ortho* Ne–H_2O in the vibrational ground state, the intermolecular states have B_1 or B_2 symmetry, which implies that intermolecular excited states in transitions to the $|02^-\rangle$ manifold must have B_1 or B_2 symmetry. The intermolecular excited states in the transitions to $|02^+\rangle$ and $|11^+\rangle$ must also have B_1 or B_2 symmetry, while the intermolecular excited states in the transition to the $|02^-\rangle$ state must have A_1 or A_2 symmetry. The formulae used to compute the line strengths have been taken from Ref. 31 in which they have been explicitly derived.

IV. RESULTS

As described above, fully converged quantum dynamical calculations have been performed on the *ab initio* 3D potential surface for Ne–H_2O, with all bound internal rotor states of *ortho*/*para* nuclear spin symmetry and *e*/*f* parity summarized in Fig. 4. Fully *ab initio* spectral predictions for the experimental overtone band with sufficient intensity to be observed can be based on the following line of thought. (i) At typical supersonic jet temperatures (10-20 K), any appreciably populated internal rotor states of Ne–H_2O must correlate asymptotically with *para* (0_{00}) and *ortho* (1_{01}) H_2O $|00^+\rangle$, with the *ortho* states favored by 3:1 nuclear spin statistics. (ii) The $v_{OH} = 2 \leftarrow 0$ stretch polyad of free H_2O has three transitions from the ground state ($|02^-\rangle \leftarrow |00^+\rangle$: $|02^+\rangle \leftarrow |00^+\rangle$: $|11^+\rangle \leftarrow |00^+\rangle$) in a rapidly decreasing

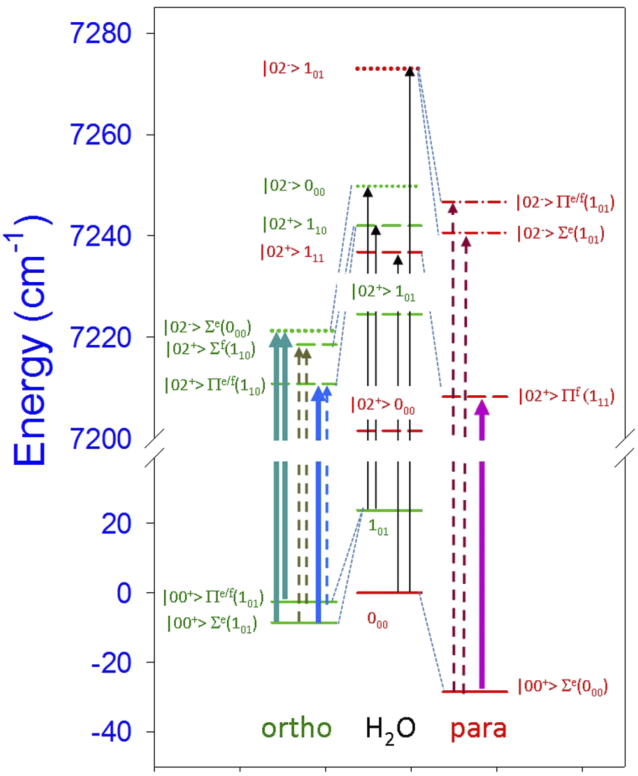

FIG. 4. Allowed IR transitions in *ortho* and *para* Ne–H_2O. H_2O is treated as a hindered asymmetric rotor with states labeled according to H_2O overtone excitation ($|02^-\rangle$ or $|02^+\rangle$), H_2O rotational state (j_{kakc}), and projection (Σ, Π) along the body fixed intermolecular cluster axis.

ratio of oscillator strengths (1.0:0.11:0.0065) that favors internal rotor transitions built on $|02^{+/-}\rangle \leftarrow |00^{+}\rangle$ and eliminates $|11^{+}\rangle \leftarrow |00^{+}\rangle$ from further consideration. (iii) Only transitions to metastable vibrational states (i.e., rigorously bound with respect to internal rotor predissociation) will be sufficiently long lived to be experimentally detected. For Ne–H_2O dissociation energies of $D_0 = 31.67\ cm^{-1}$ (*para*) or $34.66\ cm^{-1}$ (*ortho*), essentially all the bound cluster states must correlate with $j_{kakc} = 0_{00}$, 1_{01}, and 1_{10} H_2O free rotor states. The one exception is the 1_{11} internal rotor *f* parity component of *para* Ne–H_2O, which has no corresponding 0_{00} state of *f* parity and thus is dynamically bound with respect to internal rotor predissociation. (iv) Finally, any monomer state with $j > 0$ will be split by anisotropy in the potential surface into $K = j + 1$ projection states, where the internal rotor splittings in *ortho* Ne–H_2O are sufficiently small (e.g., $E_{\Pi(101)} - E_{\Sigma(101)} \approx 5.2\ cm^{-1}$) to be appreciably thermally populated under typical supersonic jet conditions.

Applying this logic to our experimental conditions, one predicts three pairs of Ne–H_2O internal rotor bands built on *ortho*-H_2O ($j_{kakc} = 1_{01}$) to be observable in the 7210-7240 cm^{-1} spectral region (se Fig. 4). The strongest pair of bands corresponds to $|02^{-}\rangle \leftarrow |00^{+}\rangle$ overtone transitions out of the most populated (*ortho*-H_2O) lower states, i.e., $|02^{-}\rangle\ \Sigma(0_{00}) \leftarrow |00^{+}\rangle\ \Sigma(1_{01})$ and $|02^{-}\rangle\ \Sigma(0_{00}) \leftarrow |00^{+}\rangle\ \Pi(1_{01})$. Based on *ab initio* internal rotor energies for the ground state and known vibrational energies of the H_2O overtone states of Tennyson *et al.*,[48] this results in predictions (solid teal) shown in Fig. 4. There will also be two additional pairs of bands built on the 9.2-fold weaker $|02^{+}\rangle \leftarrow |00^{+}\rangle$ overtone transition, the most observable of which being the overlapping Q branch feature arising from a perpendicular $\Pi \leftarrow \Sigma$ band out of the more populated (*ortho*-H_2O) ground state, i.e., $|02^{+}\rangle\ \Pi(1_{10}) \leftarrow |00^{+}\rangle\ \Sigma(1_{01})$. Relying similarly on *ab initio* Ne–H_2O internal rotor eigenvalues and literature values for the monomer overtone levels,[48] one arrives at predictions for these two additional pairs of bands marked in the left hand side of Fig. 4 by the one solid (blue) and three dotted arrows (olive and blue) for the stronger and weaker transitions, respectively. The corresponding spectroscopically predicted transitions in the *para* nuclear spin manifold are also presented in Fig. 4.

Sample IR-UV-UV spectral data over the *ortho*/*para* Ne–H_2O $v_{OH} = 2$ overtone region (7210-7240 cm^{-1}) are shown in Fig. 5, obtained by (i) tuning the infrared laser frequency, (ii) photolyzing at 193 nm after $\tau = 150$ ns, and (iii) monitoring fluorescence from high quanta end-over-end OH rotational states via the $Q_{11}(N = 8)$ transition at 309.24 nm. The long time delay between infrared and photolysis beams ensures that vibrational predissociation of the Ne–H_2O cluster species is complete before OH detection. Each feature in the spectrum is a result of vibrationally excited molecules or clusters in the supersonic jet due to IR on/off background subtraction. As expected, the spectra are dominated by overtone transitions in free H_2O monomer. However, additional contributions from Ne–H_2O clusters are clearly evident as multiple P/R and unresolved Q branch features in the spectrum, with, as we shall see, band origins in remarkable agreement with the *ab initio* theoretical predictions (solid arrows).

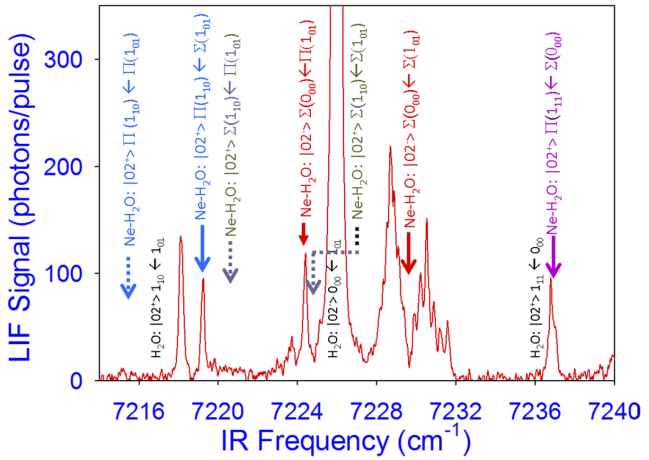

FIG. 5. Ne–H_2O vibrationally mediated photolysis (VMP) action spectra in the $v_{OH} = 2 \leftarrow 0$ overtone region, recorded as a function of infrared laser frequency while monitoring formation of highly rotationally excited OH (N = 8) products. OH is produced from Ne–H_2O based on (i) infrared excitation of the H_2O subunit followed by (ii) vibrationally mediated photolysis at 193 nm and (iii) state-specific detection of the OH(N = 8) photofragment by laser induced fluorescence (LIF). The arrows correspond to fully *ab initio* predictions from fully converged quantum theoretical calculations on a CCSD(T)-f12b/VnZ-f12 (n = 3,4), basis set superposition error (BSSE) corrected, and complete basis set (CBS) extrapolated potential energy surface (see text for details).[42,43]

More quantitatively, the strongest Ne–H_2O band at 7229.63 cm^{-1} exhibits clear $\Sigma \leftarrow \Sigma$ structure with (i) partially rotationally resolved P/R branches and (ii) absence of a Q branch, which permits it to be unambiguously assigned to the $|02^{-}\rangle\ \Sigma(0_{00}) \leftarrow |00^{+}\rangle\ \Sigma(1_{01})$ internal rotor transition in *ortho* Ne–H_2O. By way of additional confirmation, this band is slightly blue shifted from the more intense $|02^{-}\rangle\ 0_{00} \leftarrow |00^{+}\rangle\ 1_{01}$ overtone line in H_2O monomer, consistent with theoretical prediction of greater Ne-induced stabilization for the ground $\Sigma(1_{01})$ vs. first excited $\Pi(1_{01})$ internal rotor components correlating with $j_{kakc} = 1_{01}$ H_2O. Note the strong compression of rotational structure in the P vs. R branch side, characteristic of a large *increase* in the effective B rotational constant upon vibrational excitation. From the *ab initio* energy level patterns in Fig. 4, a slightly weaker $\Sigma \leftarrow \Pi$ band is also predicted and observed at 7224.40 cm^{-1}, which arises from transitions out of the corresponding first excited $\Pi(1_{01})$ internal rotor manifold. Due to finite IR pump laser resolution ($\Delta\nu \approx 0.20\ cm^{-1}$), the many overlapping transitions in the Q branch form by far the most prominent feature, but weaker P branch structure is also evident to the red, with corresponding R branch structure apparent only as a shoulder on the strong $|02^{-}\rangle\ 0_{00} \leftarrow |00^{+}\rangle\ 1_{01}$ H_2O overtone pedestal. Note that since both transitions access the same $|02^{-}\rangle\ \Sigma(0_{00})$ upper state, the spacing of these $\Sigma \leftarrow \Sigma$ and $\Sigma \leftarrow \Pi$ bands provides a direct estimate ($\Delta\nu \approx 5.2\ cm^{-1}$) for the $\Sigma - \Pi$ internal rotor splitting in the ground vibrational manifold. As evident from Fig. 4, these are the only infrared active *ortho* Ne–H_2O bands predicted from transitions built on the $|02^{-}\rangle \leftarrow |00^{+}\rangle$ H_2O monomer vibration.

A third band at 7219.25 cm^{-1} is also evident in Fig. 5 and, again based on predictions from the *ab initio*/quantum dynamics calculations, can be assigned to $\Pi(1_{10}) \leftarrow \Sigma(1_{01})$ transitions in the substantially weaker $|02^{+}\rangle \leftarrow |00^{+}\rangle$ overtone manifold. Note that the perpendicular structure for a $\Pi - \Sigma$

band yields a strong Q branch of nearly comparable intensity to the $\Sigma \leftarrow \Pi$ internal rotor band mentioned above. As all three of these bands originate from states correlating with *ortho* 1_{01} H_2O, this suggests that the 9.2-fold decrease in $|02^+\rangle \leftarrow |00^+\rangle$ vs. $|02^-\rangle \leftarrow |00^+\rangle$ overtone line strength is roughly matched by the exp(−ΔE/kT) Boltzmann factor for populating the first excited $\Pi(1_{01})$ vs. ground state $\Sigma(1_{01})$ internal rotor level. Based on an experimentally observed $\Sigma - \Pi$ internal rotor splitting of $\Delta E = 5.2\ cm^{-1}$, this would suggest a rotational temperature of $T_{rot} \approx 4$ K. It is worth noting that these rotational temperatures are more than 3× colder than typically observed ($T_{rot} \approx$ 10-20 K) in our slit jet supersonic expansions. However, as discussed in Sec. V, a cluster rotational temperature of 4 K does indeed prove to be consistent with detailed modeling of the $|02^-\rangle\ \Sigma(0_{00}) \leftarrow |00^+\rangle\ \Sigma(1_{01})$ band.

Of particular dynamical interest, a fourth internal rotor band of Ne–H_2O is evident in Fig. 5 at 7236.99 cm^{-1}, specifically as unresolved Q-branch structure on the blue side of the $|02^+\rangle \leftarrow |00^+\rangle\ 1_{11} \leftarrow 0_{00}$ overtone transition in H_2O monomer. From the *ab initio* bound state calculations, this is in excellent agreement with predictions for the $\Pi^{e/f}(1_{11}) \leftarrow \Sigma^e(0_{00})$ internal rotor band of the *para* H_2O monomer. It is worth emphasizing that the upper state of this transition is *in excess* of the internal rotor dissociation limit to form Ne + H_2O $|02^+\rangle\ 0_{00}$. What makes this particularly noteworthy is that, unlike predissociation via vibration to translation (V-T) energy transfer (which is generally negligibly slow), rotational to translational (R-T) predissociation can be extremely rapid and typically occurs on the subpicosecond time scale of a single rotational period. Such rapid predissociation would therefore be expected to result in (i) multi cm^{-1} line broadening in excess of the IR pump laser resolution and thus (ii) a strong suppression of peak absorbances. In clear contrast to these expectations, the surprisingly strong VMP signals from this upper state highlight a novel source of dynamical metastability in the $\Pi^f(1_{11})$ internal rotor manifold, which will be discussed in more detail in Sec. V.

V. DISCUSSION

A. *Ab initio* intensities

At the $\Delta\nu = 0.20\ cm^{-1}$ spectral resolution of the IR pump laser, the VMP spectra clearly exhibit both unresolved P, Q, and R branch structure and even partial rotational resolution on the strongest $|02^-\rangle\ \Sigma(00_0) \leftarrow |00^+\rangle\ \Sigma(1_{01})$ internal rotor band, which provide multiple opportunities for comparison with first principles theory. Quantum dynamical calculations on the *ab initio* Ne–H_2O intermolecular potential surface provide both (i) accurate eigenvalues for detailed frequency predictions, but also yield (ii) reliable eigenfunctions with which to calculate the intensity of a given rotationally resolved internal rotor transition.[30,32] What is especially relevant about such intensity calculations is that the intermolecular potential for Ne–H_2O is only very weakly anisotropic, and thus what may appear as relatively pure Σ and Π states for a given low J value can become strongly mixed by Coriolis coupling via end-over-end tumbling at higher J.[51–53] As a result, a parallel band (ΔK = 0) at low J can acquire partial perpendicular character (ΔK = ±1) due to rotationally mediated transition dipole moment contributions, which, in turn, can constructively augment or destructively diminish line intensities. In effect, *ab initio* frequencies *and* intensities provide the only rigorously meaningful route to a direct benchmark comparison with experiment.

B. Rotationally resolved spectra and comparison with theory

The line strengths calculated from the analysis of the *ab initio* internal rotor eigenfunctions permit one to construct a rigorous rotational band contour simulation for comparison with the experimental spectra. Specifically, we use the lower state energies and degeneracies to predict Boltzmann populations in the lower state, calculate transition frequencies from the *ab initio* energies, and smooth the resulting stick spectrum over the $\Delta\nu = 0.20\ cm^{-1}$ resolution of the IR pump laser. The result of such a comparison for the $|02^-\rangle\ \Sigma(00_0) \leftarrow |00^+\rangle\ \Sigma(1_{01})$ internal rotor band is shown in Fig. 6, which displays the most prominent rotationally resolved structure. This also allows us to adjust T_{rot} in our simulation to achieve the best visual match with experimental data, which we then treat as common to all the other rotational band contours. Particularly considering large amplitude motion and rotation-vibration Coriolis interaction in these weakly bound van der Waals clusters, the level of agreement between experiment and first principles theory for the observed rotational structure is remarkably good. In particular, the simulation successfully recapitulates both P/R branch rotational spacings, as well as the strong blue shading of the rotational structure consistent with an increase in effective rotational constant with overtone rovibrational excitation. Though even higher resolution studies would clearly be invaluable, the current data (see Table II) already justify analysis as a pseudodiatomic molecule to yield $B'_{eff} = 0.140(1)\ cm^{-1}$ and $B''_{eff} = 0.131(1)\ cm^{-1}$. Note that such a treatment predicts

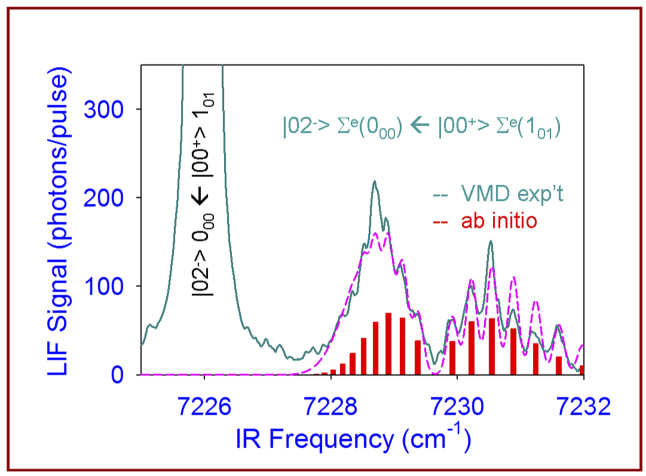

FIG. 6. Blowup of the $|02^-\rangle\ \Sigma(0_{00}) \leftarrow |00^+\rangle\ \Sigma(1_{01})$ overtone band in *ortho* Ne–H_2O, which demonstrates remarkable agreement with predictions (pink dashed line) from converged rovibrational quantum calculations of both (i) frequencies and (ii) intensities on a high level *ab initio* potential energy surface and convoluted over cluster temperature and $\Delta\nu = 0.2\ cm^{-1}$ IR laser resolution. Note that the fitted rotational temperature ($T_{rot} = 4.1(1)$ K) is significantly colder than typically observed (10-20 K) in a slit supersonic jet expansion, which from RRKM arguments suggests evaporative cooling of the Ne–H_2O clusters due to such small binding energies ($D_0 \approx$ 32-35 cm^{-1}). See text for details.

TABLE II. Vibrationally mediated photolysis rovibrational data for the $|02^-\rangle\Sigma^e(0_{00}) \leftarrow |00^+\rangle\Sigma^e(1_{01})$ band in *ortho* Ne–H_2O clusters.

Transition	Obs	Obs - Calc
P(7)	7228.184	−0.007
P(6)	7228.344	0.005
P(5)	7228.531	0.026
P(4)	7228.692	0.002
P(3)	7228.876	−0.019
P(2)	7229.089	−0.028
P(1)	7229.360	0.000
R(0)	7229.907	0.006
R(1)	7230.210	0.010
R(2)	7230.526	0.009
R(3)	7230.880	0.025
R(4)	7231.185	−0.024
R(5)	7231.578	−0.005
B''_{eff}	0.1305(6)	
B'_{eff}	0.1400(7)	
ν_0	7229.631(8)	

a substantial *increase* in rotational constant upon vibrational excitation ($\Delta B_{eff} \approx +0.009$ cm^{-1}) consistent with the blue shading observed in the experimental spectra.

For such weakly bound complexes, vibrational shifts in effective rotational constants can arise from multiple contributions. First of all, the internal rotor eigenfunction for H_2O changes its orientation in the body fixed frame upon excitation, which can either increase or decrease the vibrationally averaged Ne–H_2O separation. For weak intermolecular potentials, for example, the nodeless $\Sigma(0_{00})$ state results in a more isotropic sampling of steric effects due to the H atoms, whereas the $\Sigma(1_{01})$ state, with one angular node, is better able to align the intermolecular wavefunctions to minimize steric repulsion. However, for the $|02^-\rangle\,\Sigma(00_0) \leftarrow |00^+\rangle\,\Sigma(1_{01})$ band, this effect alone would predict a less compact structure in the upper state ($\Delta B'_{eff} < 0$), i.e., *inconsistent* with the observed blue shading.

A much larger contribution arises due to strong Coriolis coupling between the $\Sigma(1_{01})$ and $\Pi(1_{01})$ manifolds, which leads to repulsion between the uncoupled eigenvalues and makes B_{eff} for the lower or higher of the two Coriolis coupled manifolds decrease or increase, respectively. More quantitatively, the off diagonal matrix elements for $\Sigma - \Pi$ Coriolis interactions are given by $H_{12} = \beta_0\ [J(J+1)]^{1/2}$, where in the limit of weak potential anisotropy, $\beta_0 \approx 2B_{rot}$. From the second order perturbation theory,[49] therefore, one predicts J dependent shifts in energy levels by $\beta^2/\Delta E \approx (2B_{rot})^2 J(J+1)/\Delta E$. From the experimental spacing of the $\Sigma - \Pi$ band origins ($\Delta E \approx 5.3$ cm^{-1}) and $B_{rot} \approx 0.13$ cm^{-1}, this would predict $\Delta B_{eff} = +0.0135$ cm^{-1}, i.e., already in reasonable agreement with the observed shading of the P/R branch rotational contours. As a final contribution, previous studies on H_2O van der Waals complexes generally indicate a slight increase in D_0 upon OH stretch excitation, which tends to decrease the Ne–H_2O bond length and thereby further augment $\Delta B_{eff} > 0$. The current VMP data are insufficient to differentiate between these three effects, though Coriolis interactions would clearly appear to be the dominant source.

It is noteworthy that the rotational temperature obtained from such analysis is only $T_{rot} \approx 4(1)$ K. This temperature is significantly colder than the more typical 10-20 K values observed in many Ar slit supersonic jet expansion studies in our group of van der Waals complexes via high resolution infrared spectroscopy.[34,35,54] We note that these 10-20 K temperatures are achieved over a wide range of Ar backing pressures (100-500 torr), far lower than the onset of Ar clustering (>1000 torr) in the slit jet environment. These differences are considerably larger than can be attributed to Coriolis interactions influencing line strengths, as these are already explicitly included in first principles calculations of the spectra. This is, however, reminiscent of the strategy behind powerful rare gas-tagging methods in vibrational predissociation spectroscopy studies of ion clusters, which exploit the relative weakness of the He- or Ne-ion cluster interaction to achieve lowest internal temperatures.[55–59] As one possibility, therefore, we consider an "evaporative cooling" model, whereby temperature reduction occurs via selective "evaporation" of the warmer species in the Ne–H_2O distribution. In this context, the thermal Ne dissociation rate can be estimated from activated complex theory to be[60]

$$k_{evap} = \nu \exp\left(-\Delta G^{\ddagger}/kT\right) \approx \nu_{attempt} \exp\left(\Delta S^{\ddagger}/k\right) \exp\left(-\Delta H^{\ddagger}/kT\right), \quad (2)$$

where $\nu_{attempt}$ is some typical attempt frequency ($\nu \approx \nu_{VdW} \approx 22$ cm$^{-1} = 6.6 \times 10^{11}$ 1/s) for accessing the transition state. The arrival time for clusters in a Ne gas mix at the laser probe region (d ≈ 5 mm, v ≈ 1 mm/μs, and $t_{probe} \approx 5$ μs) provides the natural time window for estimating the evaporation rate, i.e., via $k_{evap}\ \tau_{probe} \approx 1$. If we assume a late transition state for evaporation behaving as essentially free Ne + H_2O subunits ($\Delta S^{\ddagger} \approx 3/2k$, $\Delta H^{\ddagger} \approx D_0 \approx 35$ cm^{-1}), Eq. (2) predicts on the order of $T_{rot} \approx 3$ K, i.e., already in reasonable agreement with experimental observation. Though a more detailed theoretical modeling would clearly be advised, this simple kinetic analysis suggests that evaporative cooling dynamics may play a significant role in temperature regulation for weakly bound cluster systems.

C. Overtone spectra in Ne–H_2O: Experiment and theory

As illustrated in Sec. V B, the availability of (i) a high quality potential energy surface and (ii) first principles quantum predictions for both frequencies and intensities of $\nu_{OH} = 2 \leftarrow 0$ overtone absorption transitions in Ne–H_2O complexes permits direct comparison between theory and experiment, even in weakly bound systems where Coriolis interactions can be predominant. By way of example, Fig. 7 presents an overview of spectral predictions for all internal rotor bands associated with *ortho* Ne–H_2O, where we have taken into account (i) Boltzmann distribution effects at $T_{rot} = 4(1)$ K for internal rotor and/or end-over-end tumbling excitation, (ii) the 0.20 cm^{-1} line width of the IR pump laser, as well as (iii) the 9.2-fold intensity difference between integrated absorption strengths for the $|02^-\rangle \leftarrow |00^+\rangle$ and $|02^+\rangle \leftarrow |00^+\rangle$ vibrational transitions.

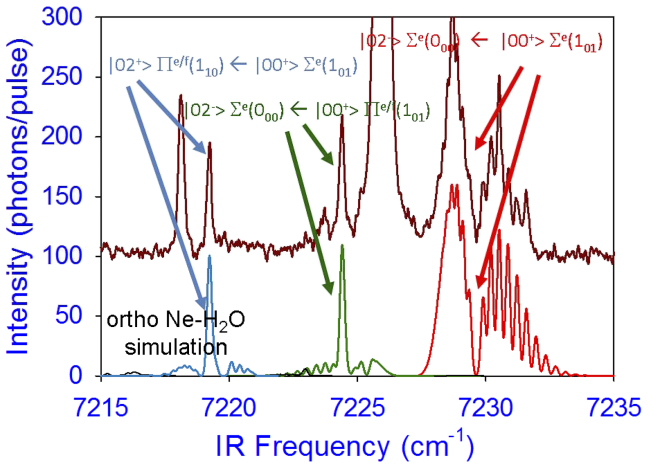

FIG. 7. Comparison of experiment with fully *ab initio* theory for vibrationally mediated photolysis (VMP) of *ortho* Ne–H_2O clusters. Note the remarkable agreement between experiment and spectral predictions based on (i) *ab initio* calculated energy levels and intensities, (ii) Boltzmann internal rotor and rotational distributions at T_{rot} = 4 K, (iii) 9.2:1 integrated intensity ratio for the $|02^-\rangle \leftarrow |00^+\rangle$ and $|02^+\rangle \leftarrow |00^+\rangle$ overtone bands, and (iv) IR pump laser linewidth of $\Delta\nu = 0.20$ cm^{-1}. The VMP features at ≈7218 cm^{-1} and ≈ 7226 cm^{-1} correspond to H_2O $|02^+\rangle$ $1_{10} \leftarrow 1_{01}$ and $|02^-\rangle$ $0_{00} \leftarrow 1_{01}$ transitions, respectively.

Immediately evident are three strong IR overtone bands features. The one band near 7229.64(2) cm^{-1} corresponds to the $|02^-\rangle\,\Sigma^e(0_{00}) \leftarrow |00^+\rangle\,\Sigma^e(1_{01})$ band analyzed and discussed previously in Sec. V B. However, also quite evident in the experimental and theoretical spectra are two much narrower features at 7224.40 cm^{-1} and 7219.25 cm^{-1}, which by comparison with the theoretical spectrum can be unambiguously assigned to unresolved Q-branch structure in the $|02^-\rangle\,\Sigma^e(0_{00}) \leftarrow |00^+\rangle\,\Pi^{e/f}(1_{01})$ and $|02^+\rangle\,\Pi^{e/f}(1_{10}) \leftarrow |00^+\rangle\,\Sigma^e(1_{01})$ internal rotor bands, respectively. The quality of the first principles predictions for the frequencies and relative intensities of the three *ortho*-Ne–H_2O band origins is remarkably good. Indeed, the results indicate only quite small deviations ($\Delta\nu \approx 0.07$–0.60 cm^{-1}) in the predicted band origins, which are most likely attributable to residual error in the *ab initio* potential surface and reduced dimensionality treatment of H_2O as a rigid asymmetric top. In addition, Fig. 7 also contains predictions for additional lower intensity overtone/internal rotor bands with band origins indicated by dashed arrows in Fig. 5. However, these transitions are below our current sensitivity levels, due either to (i) the absence of overlapping Q-branch lines for a parallel band ($\Delta K = 0$) or (ii) excitation out of an excited internal rotor state with low thermal population under such cold jet conditions (4 K).

One final point worth mentioning is that relative intensities in the VMP "*action*" spectrum for ortho Ne–H_2O complexes are very strongly correlated with predictions for the corresponding IR overtone *absorption spectrum*. That this would be the case is certainly far from obvious. Indeed, detection in our VMP "action" spectrum requires multiple additional processes to occur *after* the IR absorption event, e.g., (i) vibrational predissociation of the cluster into a distribution of quantum states, followed by (ii) quantum state selective 193 nm photolysis of the vibrationally excited H_2O, and finally (iii) UV/LIF probing a specific rotational state of the OH (typically N = 8). This remarkable correlation between predicted IR absorption and VMP action spectrum points strongly to the likelihood of a common rovibrational predissociation pathway to form Ne + *ortho* H_2O. This even higher level of dynamical information may be encoded in the pump-probe time dependent appearance as well as the nascent rotational and spin-orbit quantum state distributions for the OH photofragment species, a topic which we will address elsewhere.

D. Parity-dependent metastability in *para*-Ne–H_2O

As a parting comment and point of discussion, let us return to evidence in the *para* Ne–H_2O VMP spectra for metastable $|02^+\rangle\,\Pi^{e/f}(1_{11})$ energy levels nominally *above* the internal rotor dissociation limit to Ne + *para* H_2O $|02^+\rangle\,(0_{00})$. In the absence of any external fields, the total Hamiltonian always commutes with the true parity operator and can therefore be rigorously labeled by spectroscopic parity labels *e* or *f*, which denote states of $(-1)^J$ or $(-1)^{J+1}$ true parity, respectively. What makes this of special dynamical interest is that the $\Pi^{e/f}(1_{11})$ internal rotor manifold is ≈37 cm^{-1} above the $\Sigma^e(0_{00})$ ground state manifold, i.e., already safely in excess of the $D_0 \approx 32$ cm^{-1} dissociation energy for *para* H_2O. Thus, the $|02^+\rangle\,\Pi^e(1_{11})$ state manifold can rapidly relax via internal rotor predissociation to the $|02^+\rangle\,\Sigma^e(0_{00})$ manifold and is therefore *rigorously unbound*. However, this is not true for $\Pi^f(1_{11})$ manifold, which for any parity conserving Hamiltonian cannot relax to $\Sigma^e(0_{00})$, and thus represents a novel set of energetically unstable albeit *rigorously parity-bound* quantum states.

This relatively simple parity observation has significant dynamical consequences for Ne–H_2O spectroscopy in both the present VMP overtone efforts as well as high resolution studies of the bend/stretch fundamentals. If we neglect any V-T vibrational relaxation effects in the H_2O subunit, by simple parity and B-type dipole selection rules, *para* Ne–H_2O $|02^+\rangle \leftarrow |00^+\rangle$ excitation out of the ground $\Sigma^e(0_{00})$ state must support allowed transitions to both *bound* (i.e., $\Pi^f(1_{11})$) and *unbound* (i.e., $\Pi^e(1_{11})$) upper states on Q and P/R branch transitions, respectively. As parity-allowed internal rotor predissociation is extremely facile, particularly for such a near resonant system ($\Delta E \approx +5$ cm^{-1}), this would predict (i) laser limited Q branch transitions and yet (ii) highly predissociatively broadened P/R branch transitions. Indeed, spectroscopy and predissociation dynamics of exactly this sort were first noted in high resolution sub-Doppler IR studies of Ne–HF, Ne–DF, He–HF, and He–DF complexes, which revealed instrumentally sharp Q branches and highly broadened P/R branches for $\Pi \leftarrow \Sigma$ internal rotor excitation corresponding to $j_{HF} = 1 \leftarrow 0$ excitation of the monomer.[52,61,62] In the limit of He–HCl complexes, predissociation broadening in the P/R branches was so extreme that only instrument limited Q-branch structure could be observed.[52] Though the current VMP data are obtained at lower spectral resolution, the qualitative impact on *para* Ne–H_2O spectra should be exactly the same. Specifically, we predict the presence of Q branch transitions to metastable, *symmetry-bound* $|02^+\rangle\,\Pi^f(1_{11})$ states, with broadening limited fundamentally by vastly slower internal vibrational relaxation of the $|02^+\rangle$. Indeed, such predictions are confirmed in Fig. 5, specifically with the clear Q branch (7236.99 cm^{-1}) to the

blue of the corresponding $|02^+\rangle\ 1_{11} \leftarrow |00^+\rangle\ 0_{00}$ transition in free H_2O monomer, and in excellent agreement with band origin predictions (solid arrow) from *ab initio* and dynamics calculations.

VI. SUMMARY

Vibrational overtone spectroscopy and dynamics of weakly bound bimolecular *ortho*/*para* Ne–H_2O clusters have been probed for the first time by vibrationally mediated photolysis (VMP) methods in a supersonic jet, based on infrared excitation of the first OH stretch overtone ($v_{OH} = 2 \leftarrow 0$) polyad[51,52] for OH stretching in the water moiety. High level *ab initio* calculation of the Ne–H_2O intermolecular potential surface has been performed with the coupled cluster method (CCSD(T)-f12b/VnZ (n = 3,4)) with correlation consistent basis sets (VTZ/VQZ), explicitly correlated electron methods, values corrected for basis set superposition error (BSSE), and extrapolated to the complete basis set (CBS) limit.[42,43] These *ab initio* theoretical calculations have permitted unambiguous assignment of multiple $v_{OH} = 2 \leftarrow 0$ overtone/internal rotor bands in the *ortho* Ne–H_2O VMP action spectrum. Data on end-over-end tumbling of the cluster are clearly evident via rotational structure in the $|02^-\rangle\ \Sigma^e\ (0_{00}) \leftarrow |00^+\rangle\ \Sigma^e\ (1_{01})$ band, fits to which permit determination of effective rotational constants and a supersonic jet temperature of $T_{rot} = 4(1)$ K. This jet temperature is anomalously low and plausibly arises from "evaporative cooling" due to very weakly bound van der Waals complexes and suggests additional support for similar cooling dynamics occurring in rare gas-tagging experiments.[55–59] Furthermore, evidence is presented for novel *e*/*f parity-dependent* internal rotor metastability in *para* Ne–H_2O clusters, due to the energetic inaccessibility of outgoing channels with the requisite *f*-parity in the H_2O subunit. Most importantly, the *ab initio* calculations provide first principles predictions of line-by-line spectra, which are in remarkable agreement with the experimental band origins and rotational band contours. The results reveal a surprising wealth of novel overtone spectroscopy and dynamics in a prototypical weakly bound van der Waals cluster, with a successful analysis facilitated by and indeed requiring close interaction between experiment and high level theory.

ACKNOWLEDGMENTS

This work was supported by grants from the Department of Energy, Office of Basic Energy Sciences (No. DE-FG02-09ER16021), with additional funds for photolysis laser and construction of the vacuum chamber provided by the Air Force Office of Scientific Research (No. FA9550-12-1-0139). J.L. is supported by the Belgian Fund for Scientific Research-FNRS. A.v.d.A. and D.J.N. also both wish to gratefully acknowledge additional assistance through the Senior Alexander von Humboldt Research Award program for providing the opportunity to work together.

[1] C. B. Anfinsen, Science **181**, 223 (1973).
[2] K. Autumn, M. Sitti, Y. C. A. Liang, A. M. Peattie, W. R. Hansen, S. Sponberg, T. W. Kenny, R. Fearing, J. N. Israelachvili, and R. J. Full, Proc. Natl. Acad. Sci. U. S. A. **99**, 12252 (2002).
[3] A. Nicholls, K. A. Sharp, and B. Honig, Proteins **11**, 281 (1991).
[4] T. Welton, Chem. Rev. **99**, 2071 (1999).
[5] R. C. Cohen and R. J. Saykally, J. Chem. Phys. **98**, 6007 (1993).
[6] R. E. Grisenti, W. Schollkopf, J. P. Toennies, G. C. Hegerfeldt, T. Kohler, and M. Stoll, Phys. Rev. Lett. **85**, 2284 (2000).
[7] P. G. Sennikov, S. K. Ignatov, and O. Schrems, ChemPhysChem **6**, 392 (2005).
[8] S. D. Flynn, D. Skvortsov, A. M. Morrison, T. Liang, M. Y. Choi, G. E. Douberly, and A. F. Vilesov, J. Phys. Chem. Lett. **1**, 2233 (2010).
[9] S. A. Nizkorodov, M. Ziemkiewicz, D. J. Nesbitt, and A. E. W. Knight, J. Chem. Phys. **122**, 194316 (2005).
[10] V. Vaida, J. Chem. Phys. **135**, 020901 (2011).
[11] N. Kobko, M. Marianski, A. Asensio, R. Wieczorek, and J. J. Dannenberg, Comput. Theor. Chem. **990**, 214 (2012).
[12] Y. A. Dyadin, E. G. Larionov, A. Y. Manakov, F. V. Zhurko, E. Y. Aladko, T. V. Mikina, and V. Y. Komarov, Mendeleev Commun. **5**, 209 (1999).
[13] F. Daniel, M. L. Dubernet, and A. Grosjean, Astron. Astrophys. **536**, A76 (2011).
[14] A. Faure, L. Wiesenfeld, Y. Scribano, and C. Ceccarelli, Mon. Not. R. Astron. Soc. **420**, 699 (2012).
[15] B. H. Yang, M. Nagao, W. Satomi, M. Kimura, and P. C. Stancil, Astrophys. J. **765**, 77 (2013).
[16] G. T. Fraser, F. J. Lovas, R. D. Suenram, and K. Matsumura, J. Mol. Spectrosc. **144**, 97 (1990).
[17] R. Lascola and D. J. Nesbitt, J. Chem. Phys. **95**, 7917 (1991).
[18] D. F. Plusquellic, O. Votava, and D. J. Nesbitt, J. Chem. Phys. **101**, 6356 (1994).
[19] J. Van Wijngaarden and W. Jager, Mol. Phys. **98**, 1575 (2000).
[20] M. J. Weida and D. J. Nesbitt, J. Chem. Phys. **106**, 3078 (1997).
[21] J. P. Lei, Y. Z. Zhou, D. Q. Xie, and H. Zhu, J. Chem. Phys. **137**, 224314 (2012).
[22] A. Bagno, J. Chem. Soc., Faraday Trans. **94**, 2501 (1998).
[23] M. P. Hodges, R. J. Wheatley, and A. H. Harvey, J. Chem. Phys. **117**, 7169 (2002).
[24] J. Makarewicz, J. Chem. Phys. **129**, 184310 (2008).
[25] D. Hou, Y.-T. Ma, X.-L. Zhang, and H. Li, J. Mol. Spectrosc. **330**, 217 (2016).
[26] S. Li, R. Zheng, Y. Zhu, and C. X. Duan, J. Chem. Phys. **135**, 134304 (2011).
[27] X. Sun, Y. Hu, and H. Zhu, J. Chem. Phys. **138**, 204312 (2013).
[28] O. Dopfer, D. Roth, and J. P. Maier, J. Chem. Phys. **114**, 7081 (2001).
[29] X. G. Wang and T. Carrington, J. Chem. Phys. **134**, 044313 (2011).
[30] M. J. Weida and D. J. Nesbitt, J. Chem. Phys. **110**, 156 (1999).
[31] M. P. Ziemkiewicz, C. Pluetzer, D. J. Nesbitt, Y. Scribano, A. Faure, and A. van der Avoird, J. Chem. Phys. **137**, 084301 (2012).
[32] A. van der Avoird and D. J. Nesbitt, J. Chem. Phys. **134**, 044314 (2011).
[33] R. N. Zare, *Angular Momentum: Understanding Spatial Aspects in Chemistry and Physics* (John Wiley & Sons, New York, 1988).
[34] C. M. Lovejoy and D. J. Nesbitt, J. Chem. Phys. **91**, 2790 (1989).
[35] C. M. Lovejoy, M. D. Schuder, and D. J. Nesbitt, J. Chem. Phys. **86**, 5337 (1987).
[36] M. S. Child and R. T. Lawton, Faraday Discuss. Chem. Soc. **71**, 273 (1981).
[37] M. S. Child, Acc. Chem. Res. **18**, 45 (1985).
[38] O. Votava, D. F. Plusquellic, and D. J. Nesbitt, J. Chem. Phys. **110**, 8564 (1999).
[39] D. F. Plusquellic, O. Votava, and D. J. Nesbitt, J. Chem. Phys. **107**, 6123 (1997).
[40] S. A. Nizkorodov, M. Ziemkiewicz, T. L. Myers, and D. J. Nesbitt, J. Chem. Phys. **119**, 10158 (2003).
[41] H.-J. Werner, P. J. Knowles, R. Lindh, F. R. Manby, M. Schütz, P. Celani, T. Korona, A. Mitrushenkov, G. Rauhut, T. B. Adler, R. D. Amos, A. Bernhardsson, A. Berning, D. L. Cooper, M. J. O. Deegan, A. J. Dobbyn, F. Eckert, E. Goll, C. Hampel, G. Hetzer, T. Hrenar, G. Knizia, C. Köppl, Y. Liu, A. W. Lloyd, R. A. Mata, A. J. May, S. J. McNicholas, W. Meyer, M. E. Mura, A. Nicklaß, P. Palmieri, K. Pflüger, R. Pitzer, M. Reiher, U. Schumann, H. Stoll, A. J. Stone, R. Tarroni, T. Thorsteinsson, M. Wang, and A. Wolf, MOLPRO, version 2009.1, a package of *ab initio* programs, 2009, see http://www.molpro.net.
[42] K. A. Peterson, T. B. Adler, and H.-J. Werner, J. Chem. Phys. **128**, 084102 (2008).
[43] K. A. Peterson, R. A. Kendall, and T. H. Dunning, J. Chem. Phys. **99**, 1930 (1993).
[44] K. A. Peterson, D. E. Woon, and T. H. Dunning, J. Chem. Phys. **100**, 7410 (1994).
[45] E. T. Whittaker and G. N. Watson, *A Course in Modern Analysis*, 4th ed. (Cambridge University Press, Cambridge, England, 1990).

[46]J. Loreau and A. van der Avoird, J. Chem. Phys. **143**, 184303 (2015).
[47]J. Loreau, J. Lievin, Y. Scribano, and A. van der Avoird, J. Chem. Phys. **141**, 224303 (2014).
[48]J. Tennyson, N. F. Zobov, R. Williamson, O. L. Polyansky, and P. F. Bernath, J. Phys. Chem. Ref. Data **30**, 735 (2001).
[49]P. R. Bunker and P. Jensen, *Molecular Symmetry and Spectroscopy*, 2nd ed. (NRC Research Press, Ottawa, 1998).
[50]H.-J. Werner, P. J. Knowles, G. Knizia, F. R. Manby, M. Schütz, and others, MOLPRO, a package of *ab initio* programs, see http://www.molpro.net.
[51]C. M. Lovejoy and D. J. Nesbitt, Chem. Phys. Lett. **147**, 490 (1988).
[52]C. M. Lovejoy and D. J. Nesbitt, J. Chem. Phys. **93**, 5387 (1990).
[53]C. M. Lovejoy and D. J. Nesbitt, J. Chem. Phys. **94**, 208 (1991).
[54]C. M. Lovejoy and D. J. Nesbitt, Rev. Sci. Instrum. **58**, 807 (1987).
[55]H. K. Gerardi, A. F. DeBlase, X. G. Su, K. D. Jordan, A. B. McCoy, and M. A. Johnson, J. Phys. Chem. Lett. **2**, 2437 (2011).
[56]C. J. Johnson, A. B. Wolk, J. A. Fournier, E. N. Sullivan, G. H. Weddle, and M. A. Johnson, J. Chem. Phys. **140**, 221101 (2014).
[57]P. J. Kelleher, C. J. Johnson, J. A. Fournier, M. A. Johnson, and A. B. McCoy, J. Phys. Chem. A **119**, 4170 (2015).
[58]M. A. Duncan, J. Phys. Chem. A **116**, 11477 (2012).
[59]J. D. Mosley, J. W. Young, M. Huang, A. B. McCoy, and M. A. Duncan, J. Chem. Phys. **142**, 114301 (2015).
[60]P. L. Houston, *Chemical Kinetics and Reaction Dynamics* (McGraw-Hill, New York, 2001).
[61]D. C. Clary, C. M. Lovejoy, S. V. Oneil, and D. J. Nesbitt, Phys. Rev. Lett. **61**, 1576 (1988).
[62]S. V. Oneil, D. J. Nesbitt, P. Rosmus, H. J. Werner, and D. C. Clary, J. Chem. Phys. **91**, 711 (1989).